scientific reports

Check for updates

OPEN

Lysyl-tRNA synthetase 1 promotes atherogenesis via autophagy-related secretion and inflammation

Kangmin Yun[1,6], Youngsik Seo[1,6], Yerim Oh[1], Sunghyen Kim[1], Hye Sun Maeng[1], Jin Gu Cho[1], Young Bae Son[2], Dong Ju Son[2], Kihwan Kwon[3], Sunghoon Kim[4], Hanjoong Jo[5] & Heonyong Park[1]✉

Lysyl-tRNA synthetase 1 (KARS1), an aminoacyl-tRNA synthetase, was recently identified as a secreted pro-inflammatory agent. However, the vascular secretion and functions of KARS1 have not been characterized. This study investigated the secretion mechanisms of KARS1 and explored its functional roles in vascular biology. We found that KARS1 expression was upregulated by oscillatory shear stress, an atherogenic factor, suggesting the presence of free KARS1 dissociated from aminoacyl-tRNA synthetase complexes. Moreover, in the presence of Ca^{2+}, serum starvation triggered free cytosolic KARS1 release from endothelial cells via secretory autophagy. Both phosphatidylinositol 3-phosphate kinase and caveolin-1 were either supplementary or essential for KARS1 secretion. Secreted KARS1 co-localized in the exosome fraction of post-culture media and was externally exposed. Further, secreted KARS1 inhibited shear-induced activation of various signaling molecules, including extracellular signal-regulated kinase, protein kinase B, and endothelial nitric oxide synthetase. Secreted KARS1 in atherosclerotic plaques also acted as an atherogenic or proinflammatory autocrine/paracrine molecule. Additionally, KARS1 participated in vessel alteration. Collectively, these findings describe novel vascular features of KARS1 in response to shear stress, providing insights into shear stress-controlling mechanisms of the vascular system.

Keywords KARS1, Secretory autophagy, Laminar shear stress, Oscillatory shear stress, Vessel alteration, Cell apoptosis

Lysyl-tRNA synthetase 1 (KARS1) is an aminoacyl-tRNA synthetase (ARS) that catalyzes the aminoacylation of cognate tRNA via ATP consumption[1]. Recent studies have revealed multiple functions of KARS1 in various cellular and molecular processes, including human immunodeficiency virus type 1 viral packaging[2], Ap_4A-controlled gene regulation in the nucleus[3–5], inflammation[6], and laminin-dependent cell migration[7]. The multifunctional activities of KARS1 are closely associated with alterations in its cellular localization[5,6]. In mammals, nine ARSs, including KARS1, form a multi-synthetase complex (MSC) in the cytosolic fraction[8] that is likely critical in improving protein synthesis efficiency through adjacent tRNA aminoacylation[9,10]. However, to perform other nuclear or extracellular functions, KARS1 dissociates from the MSC and translocates to other relevant locations. Alternatively, KARS1 overexpression enhances the possibility of its dissociation from the MSC. Therefore, the extracellular vascular functions of KARS1 arise either from its dissociation from the MSC or from the presence of its free form in the cytosol due to overexpression.

The translational activity of KARS1 occurs in the cytoplasm. However, KARS1 is extracellularly secreted from the cytosol, allowing it to function in an autocrine/paracrine manner. As KARS1 lacks a signal sequence, it is not secreted via the canonical ER–Golgi–plasma membrane trafficking system. Moreover, secreted KARS1

[1]Department of Molecular Biology, Institute of Nanosensor and Biotechnology, Dankook University, 119 Dandae-Ro, Dongnam-Gu, Cheonan-Si, Chungnam 31116, South Korea. [2]College of Pharmacy, Chungbuk National University, 194-21 Osongsaengmyong 1-Ro, Osong-Eup, Heungduk-Gu, Cheongju 28160, Chungbuk, Republic of Korea. [3]Division of Cardiology, Department of Internal Medicine, Ewha Womans University College of Medicine, Ewha Womans University Mokdong Hospital, Seoul, Republic of Korea. [4]Department of Integrative Biotechnology, Interdisciplinary Graduate Program, Medicinal Bioconvergence Research Center, Institute for Artificial Intelligence and Biomedical Research, College of Pharmacy, Yonsei University, 85 Songdogwahak-Ro, Yeonsu-Gu, Incheon 21983, Korea. [5]Wallace H. Coulter Department of Biomedical Engineering, Georgia Institute of Technology and Emory University, Atlanta, GA, USA. [6]Kangmin Yun, Youngsik Seo These authors contributed equally to this work. ✉email: heonyong@dankook.ac.kr

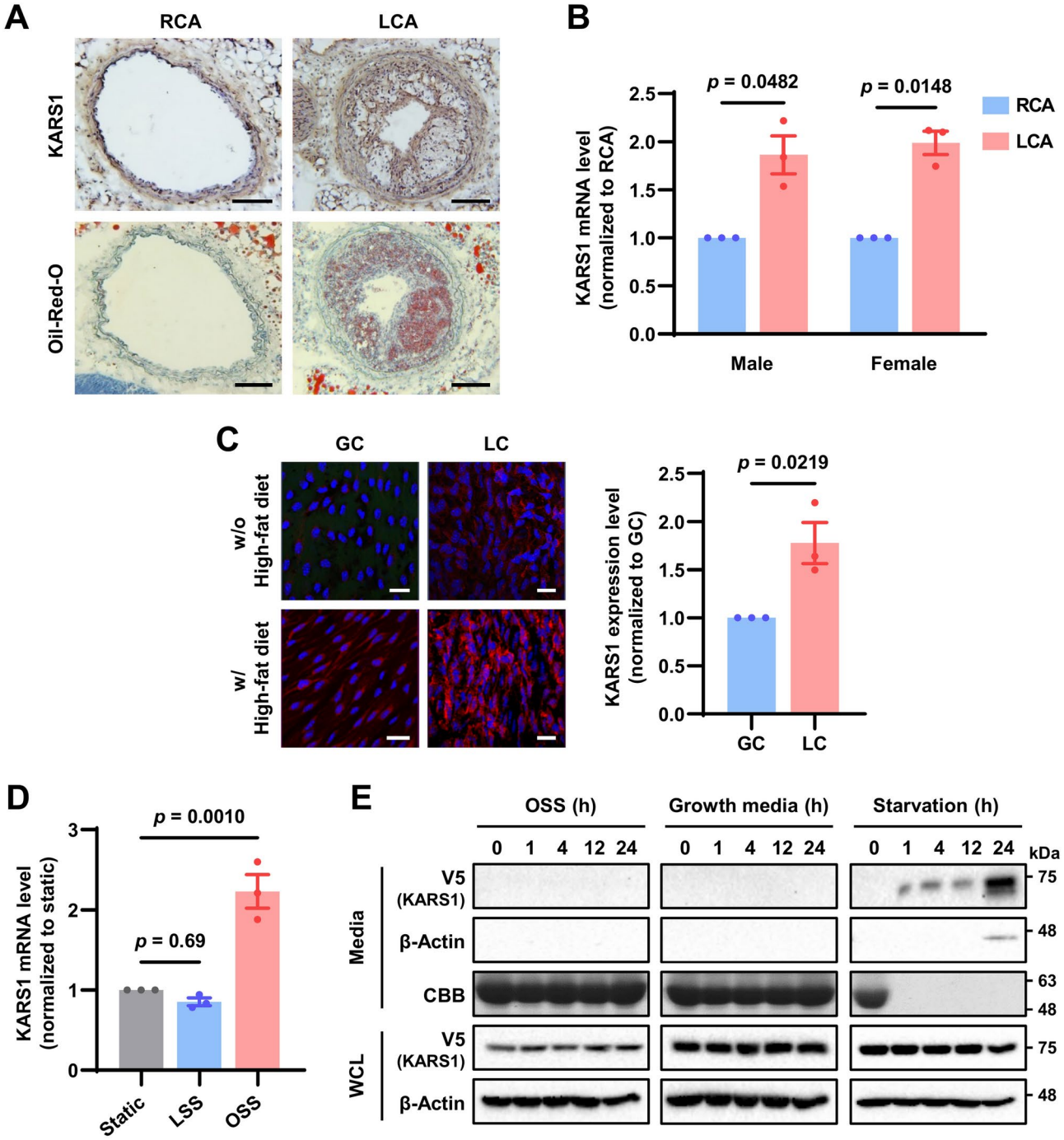

binds directly to macrophages[6], suggesting that it is externally exposed. Recently, novel secretory pathways for cytosolic proteins involving amphisomes, closely associated with autophagy, have been proposed[11]. Colorectal cancer cells reportedly secrete KARS1 in exosomes[12]. Meanwhile, serum starvation—a well-known autophagy stimulator—consistently induces KARS1 secretion from cancer cells[12]. This suggests that KARS1 secretion may be associated with autophagy. However, the detailed mechanisms underlying KARS1 secretion require further investigation.

KARS1 secretion into extracellular spaces is stimulated by tumor necrosis factor (TNF)-α in HCT116 colon cancer cells, activating immune cells[6]. This suggests that KARS1 acts as a pro-inflammatory factor. Pro-inflammatory factors promote atherogenesis[13,14]. A representative pro-atherogenic factor is oscillatory shear stress (OSS), whereas laminar shear stress (LSS) is anti-atherogenic[15]. Shear stress is generated by frictional forces between the endothelium, the innermost single layer of blood vessels, and blood. LSS occurs in vessels exposed to unidirectional and streamlined blood flow, whereas OSS is generated by blood flow in alternate directions. Atherosclerotic plaques are frequently found in vessels exposed to OSS or low LSS[15]. Indeed, endothelial cells respond differently to OSS and LSS.

LSS activates various cell signaling pathways in endothelial cells through extracellular signal-regulated kinase (ERK), c-Jun N-terminal kinase, protein kinase B (AKT), and endothelial nitric oxide synthase (eNOS)[16,17].

◀**Fig. 1**. Lysyl-tRNA synthetase 1 (KARS1) is overexpressed by oscillatory shear stress (OSS) and secreted by serum starvation in endothelial cells. **A.** Immunohistochemistry staining shows KARS1 expression level in the partially ligated carotid artery of Apolipoprotein E knock-out (ApoE KO) mice fed a high-fat diet for two weeks. The right carotid artery (RCA) was normal and the left carotid artery (LCA) was ligated. The lipids were stained red with oil-red-O. Nuclei were counterstained with hematoxylin. Representative images are shown ($n = 6$). Scale bar = 100 μm. **B.** KARS1 mRNA levels analyzed by qPCR in the partially ligated carotid arteries of C57BL/6 mice fed a high-fat diet for two weeks. The data were statistically analyzed using Student's *t*-test ($n = 3$, each). **C.***En face* staining of the greater curvature (GC) and lesser curvature (LC) of the aortic arch in ApoE KO mouse tissue stained with an anti-KARS1 antibody (left panel). Nuclei were counterstained with DAPI. Representative images are presented ($n = 3$). Scale bar = 50 μm. KARS1 fluorescence intensity in the high-fat diet group quantified and analyzed using Student's *t*-test (right panel). **D.** Bovine aortic endothelial cells (BAECs) were pre-treated with laminar shear stress (LSS) or OSS for 2 h. KARS1 mRNA levels were analyzed by qPCR. Static was a non-shear stress control. Data were statistically analyzed using one-way analysis of variance (ANOVA), followed by Tukey's honest significant difference (HSD) test ($n = 3$). **E.** BAECs were transfected with a vector containing the *KARS1* gene tagged with *V5*. Western blots for post-culture media and whole-cell lysates (WCL) of BAECs treated with OSS, growth media, and under serum starvation. CBB: Coomassie Brilliant Blue. β-Actin is the loading control. Representative blots are shown ($n = 3$). All bar graphs are presented as mean ± SEM.

These signaling molecules regulate myriad cellular processes, including proliferation and apoptosis, that ultimately impact the vascular system[18,19]. However, a relative paucity of data is available regarding how LSS/OSS-induced activation of signaling molecules directly or indirectly impacts vascular activities and diseases. In contrast, nitric oxide (NO) is a well-known gasotransmitter that regulates vascular functions. In fact, reduced NO levels throughout the vascular system cause major cardiovascular diseases, such as arterial hypertension and dyslipidemia[20]. Meanwhile, LSS and OSS have been shown to regulate NO production, modulating the vascular system to maintain vascular health[21]. Specifically, shear stress controls basal vascular tone, endothelial cell survival, and angiogenesis via NO regulation[22].

Given KARS1's pro-inflammatory function and, thus, potential atherogenic effect, this study sought to elucidate the vascular role of KARS1. In particular, this study aimed to evaluate how KARS1, when overexpressed and not incorporated into the MSC, is secreted extracellularly and exerts its vascular functions. Moreover, to clarify the vascular secretion of cytosolic KARS1 in the absence of a signal sequence and specific membrane transporter system, we aimed to investigate the detailed molecular mechanisms of KARS1 secretion and assess the potential involvement of various vesicular transport systems. Furthermore, this study aimed to provide novel insights into KARS1-associated shear activation of various cell signaling molecules in the vascular system, with potential implications for vascular remodeling.

Results

KARS1 expression is enhanced by OSS

We first examined whether KARS1 expression is modulated in an in vivo OSS model induced by partial ligation. Through partial ligation of the left carotid artery (LCA) of Apolipoprotein E knock-out (ApoE KO) mice, OSS-like disturbed flow was induced in the LCA, while the intact right carotid artery (RCA) was exposed to LSS-like shear stress. After partial ligation, KARS1 expression was monitored, revealing upregulation of KARS1 mRNA and protein levels in LCA, with marked atheroma (Fig. 1A–B). This supports the hypothesis that OSS upregulates KARS1 expression. To test this hypothesis further by alternative in vivo experiments, we performed *en face* staining of the greater and less curved aortic arch with an anti-KARS1 antibody. The greater curvature (GC) is exposed to LSS-like blood flow, whereas the lesser curvature (LC) is exposed to OSS-like blood flow[23]. The fluorescence intensity of KARS1 (red) in the LC was higher than that in the GC (Fig. 1C).

We then tested whether shear stress affects KARS1 in vitro expression. The expression of KARS1 mRNA gradually increased with extended OSS exposure in bovine aortic endothelial cells (BAECs) and mouse aortic endothelial cells (MAECs). In contrast, LSS treatment induced no changes in KARS1 mRNA expression (Fig. 1D and Supplementary Fig. 1A–B). Other conditions (serum starvation, TNF-α (apoptotic and pro-inflammatory agent), lipopolysaccharide (LPS, pro-inflammatory agent), and resveratrol (RSV, apoptotic agent)) did not appear to affect the expression of KARS1 (Supplementary Fig. 1C). These findings suggest that KARS1 overexpression occurs in the vascular system under exposure to OSS, an atherogenic stimulus.

Serum starvation and intracellular Ca^{2+} induce KARS1 secretion by endothelial cells

To determine whether endothelial cells secrete overexpressed KARS1, BAECs were treated with various endothelial regulators, including OSS, TNF-α, LPS, and RSV. Among these regulators, serum starvation induced KARS1 secretion by endothelial cells (Fig. 1E and Supplementary Fig. 1D–F).

To assess whether KARS1 secretion is regulated by intracellular [Ca^{2+}]—a well-known secondary messenger for exocytosis—BAECs were treated with A23187, a calcium ionophore. This promoted KARS1 secretion; however, the effect of Ca^{2+} on KARS1 secretion was inhibited by the calcium chelator, EGTA/AM (Fig. 2A and Supplementary Fig. 2A). These results confirmed that intracellular Ca^{2+} induced KARS1 secretion. Meanwhile, treatment with Exo-1—an exocytosis inhibitor—did not affect KARS1 secretion (Fig. 2B and Supplementary Fig. 2B), indicating that Ca^{2+}-induced KARS1 secretion was not associated with exocytosis.

KARS1 overexpression altered the phosphorylation of AMP-activated protein kinase (AMPK) and phosphoinositide 3-kinase (PI3K) among autophagy-related signaling proteins (Fig. 2C and Supplementary

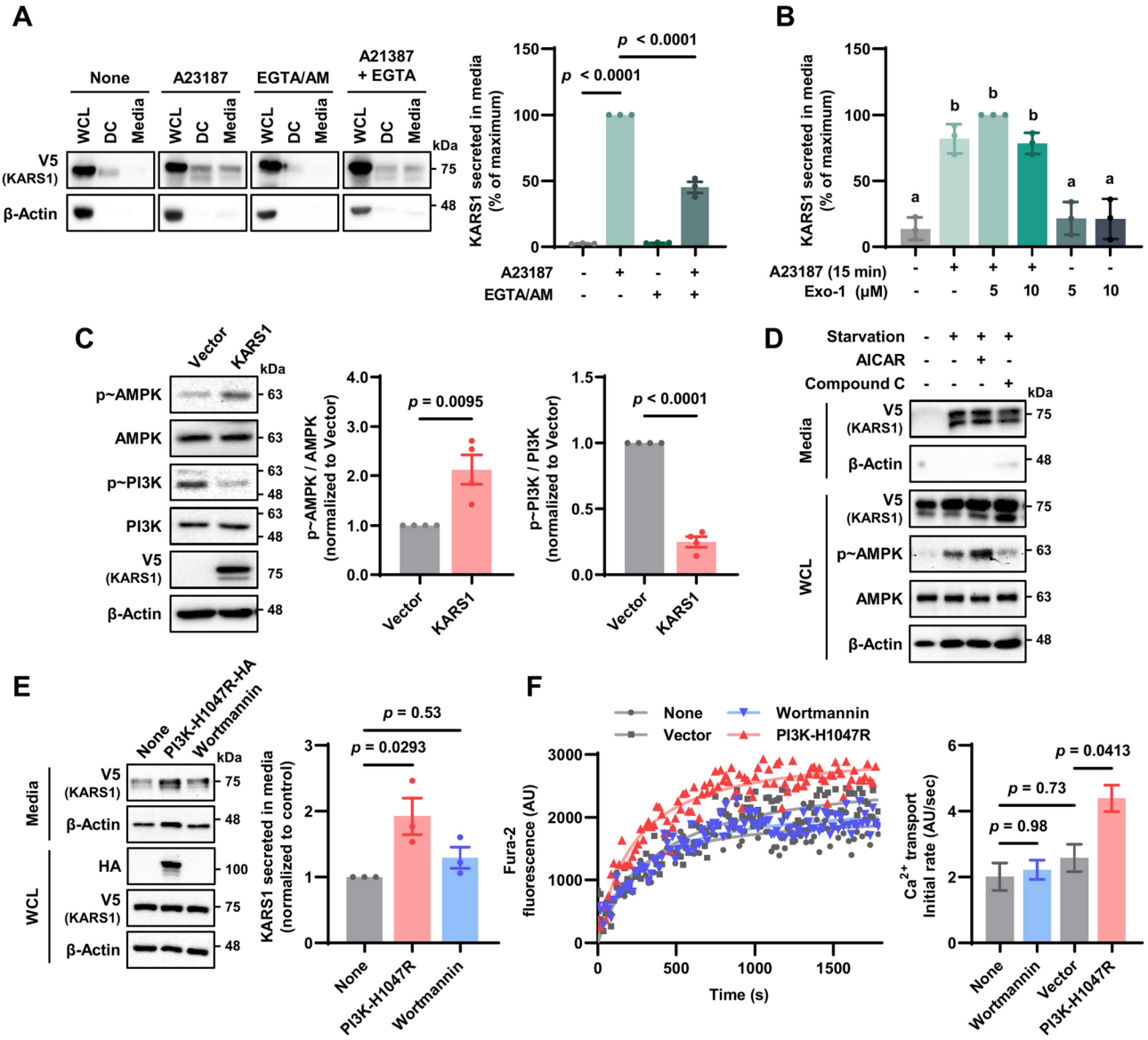

Fig. 2. Lysyl-tRNA synthetase 1 (KARS1) secretion is stimulated by cytosolic Ca^{2+} in endothelial cells. **A.** Bovine aortic endothelial cells (BAECs) were transfected with a vector containing the *KARS1* gene tagged with *V5* and serum-starved for 24 h. Western blotting (left panel) of whole-cell lysates (WCL), suspended dead cells (DC), and post-culture media obtained from BAECs treated with 1 μM A23187 and/or 100 μM EGTA/AM. β-Actin is the loading control. Representative blots are shown ($n = 3$). KARS1 blots were quantified using densitometry and analyzed using two-way analysis of variance (ANOVA), followed by Sidak's correction (right panel). **B.** BAECs, after transfection with the vector carrying *KARS1-V5* and 24 h serum starvation, were treated with 1 μM A23187 and/or Exo-1 for 15 min. Quantified blot data were analyzed using ANOVA, followed by Tukey's honest significant difference (HSD) test ($n = 3$). **C.** Western blotting (left panel) was performed on WCL from BAECs transfected with an empty vector or a vector carrying *KARS1-V5* and serum-starved for 24 h. Representative blots are shown ($n = 4$). Quantified blot data (right panels) analyzed using Student's *t*-test. **D–E.** BAECs, after transfection of vector with *KARS1-V5* and 24 h serum starvation, were treated with 500 μM AICAR or 10 μM Compound C (**D**). BAECs were transfected with a vector carrying *PI3K-H1047R* or treated with 10 nM wortmannin (**E**). Representative blots are shown ($n = 3$). Quantified blot data (right panel of E) were analyzed using one-way ANOVA followed by Tukey's HSD test. **F.** Fura-2 fluorescence intensities were monitored for 30 min at 17-s intervals, starting 30 min after the media was changed from phosphate buffered saline to serum-starved media (left panel). The initial rates, represented by the slopes, are replotted as bar graphs (right panel). Slopes analyzed using a one-way ANOVA, followed by Tukey's HSD test. All bar graphs are presented as mean ± SEM.

Fig. 2C), but did not directly affect calcium influx (Supplementary Fig. 2D–E). More specifically, AMPK phosphorylation was increased by KARS1 overexpression; however, this effect did not impact KARS1 secretion (Fig. 2D). In contrast, PI3K was dephosphorylated upon KARS1 overexpression and was primarily associated with KARS1 secretion (Fig. 2E). The constitutively active PI3K-H1047R mutant appeared to promote KARS1 secretion by 1.5-fold and Ca^{2+} influx by twofold (Fig. 2F and Supplementary Fig. 2F). In contrast, the PI3K inhibitor, wortmannin, did not affect Ca^{2+} influx or KARS1 secretion. This may be attributed to the marginally low intracellular Ca^{2+} concentration under our cell culture conditions. Accordingly, an increase in intracellular Ca^{2+} is functionally significant for KARS1 secretion, whereas a decrease exerts no substantial effect.

Ectopically overexpressed KARS1 is secreted in association with exosomes

To determine whether overexpressed (ectopic) KARS1 is secreted by exosomes, exosomes were prepared using multiple independent methods. With ultra-centrifugal fractionation, KARS1 secretion was associated with exosomes during serum starvation, but not in growth media (Fig. 3A and Supplementary Fig. 3). Consistently, A23187 increased both KARS1 and CD63 (exosome marker) secretion (Fig. 3B). Moreover, sucrose gradient fractionation showed that secreted KARS1 was present in fractions containing CD63, whereas recombinant KARS1 protein was found in the lower (high-density) fractions. This indicated that secreted KARS1 was bound or incorporated into lipid-containing vesicles (Fig. 3C). Additional exosome preparation confirmed that KARS1 protein was present in the exosome fraction (Fig. 3D).

We then investigated whether a portion or the entire secreted KARS1 molecule was exposed on the surface of exosomes using co-immunoprecipitation (co-IP) with an anti-V5-tag antibody. IP with anti-V5 antibodies showed that CD63 was not co-immunoprecipitated in the exosome fraction, as evidenced by CD63 remaining in the IP remnant relative to the amount of input (Fig. 3E). Accordingly, we speculated that (1) KARS1 was exposed on the surface of the exosome, and (2) KARS1 interacts with the exosome to form a complex, but is not inserted into the exosome.

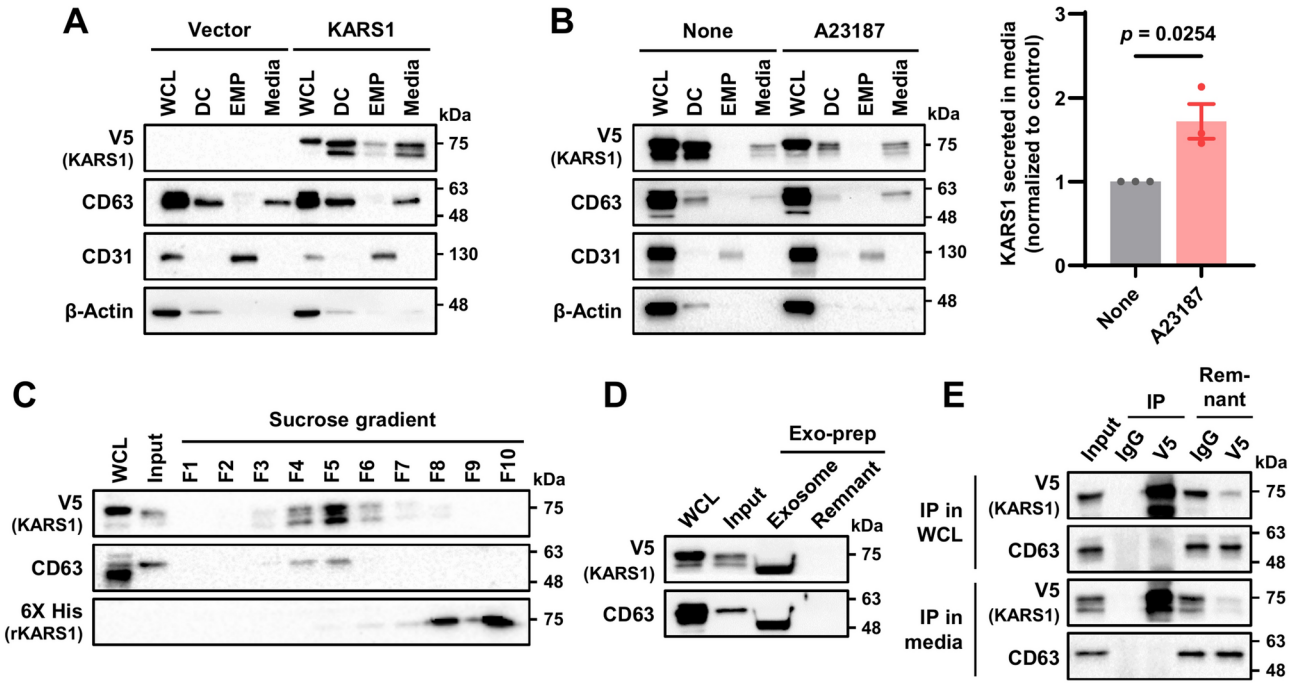

Fig. 3. Ectopically overexpressed lysyl-tRNA synthetase 1 (KARS1) is secreted as exosome-associated complexes. **A–B.** Bovine aortic endothelial cells (BAECs) were transfected with an empty vector or a vector containing the *KARS1* gene tagged with *V5* and serum-starved for 24 h. In (**B**), transfected cells were treated with or without 1 μM A23187 for 15 min. The post-culture media were fractionated by ultracentrifugation steps: DC, suspended dead cells; EMP, endothelial microparticles; and media, exosome fractions. Western blotting was performed on whole-cell lysates (WCL) and fractionated media. β-Actin is the loading control. Representative blots are shown ($n = 3$). Data were analyzed using Student's *t*-test. **C.** Each fraction (F1–10) from the sucrose gradient fractionation of BAECs and recombinant KARS1 protein (His-tagged rKARS1) were immunoblotted. **D.** Exosomes were prepared by collecting culture media from BAECs transfected with a vector carrying *KARS1-V5*. Input, post-culture media before exosome preparation; Remnant, non-exosomal fraction. Representative blots are shown ($n = 3$). **E.** Co-immunoprecipitation using anti-V5 antibody and subsequent western blotting. BAECs were transfected with a vector carrying *KARS1-V5*. Representative blots are shown ($n = 3$).

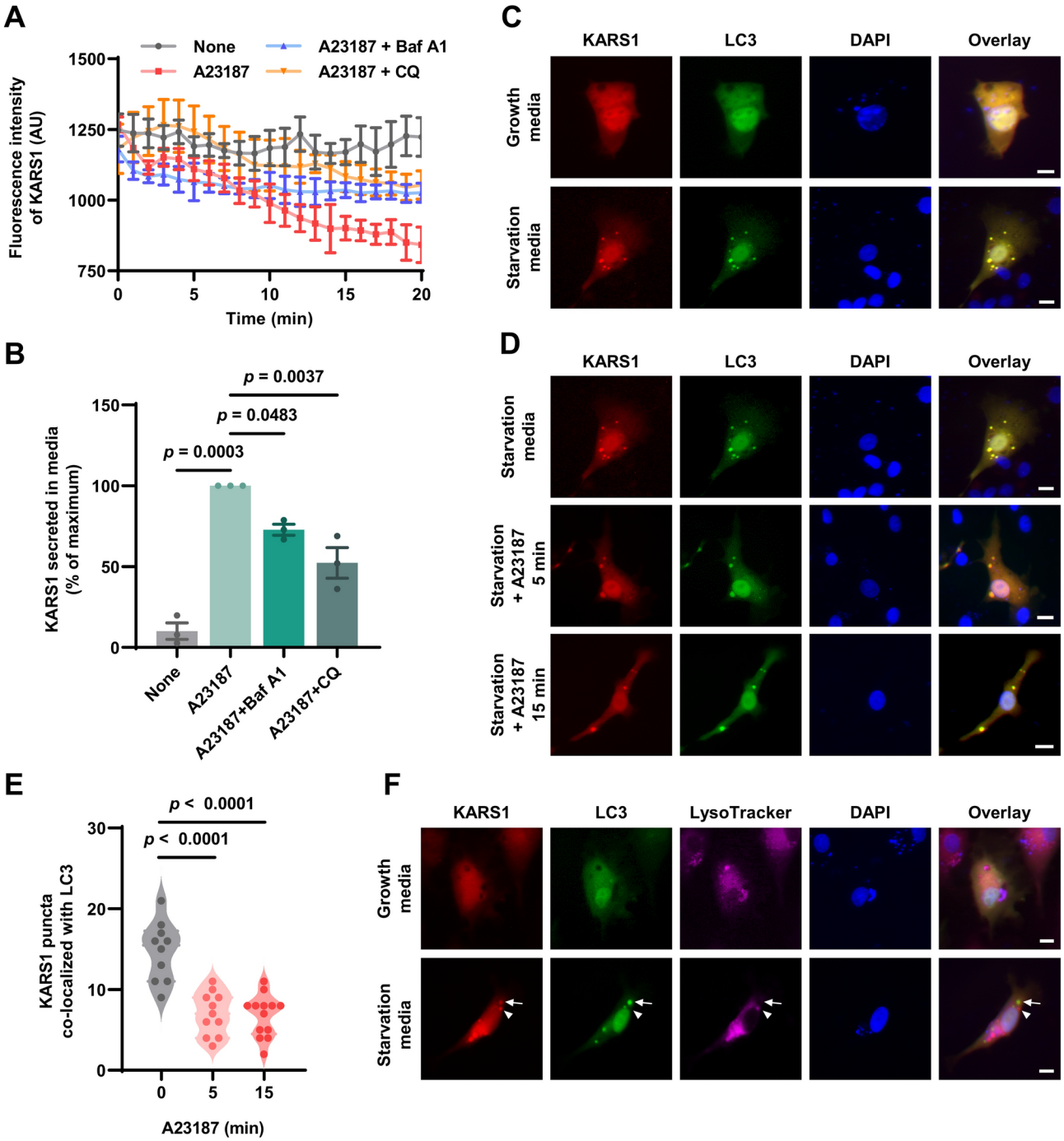

KARS1 is secreted through autophagy

To determine whether KARS1 secretion is associated with serum starvation-induced autophagy, BAECs were transfected with a vector containing the gene encoding C-terminal red fluorescent protein (*RFP*)-tagged *KARS1* (KARS1-RFP) and then treated with A23187 or the autophagy inhibitors bafilomycin A1 (Baf A1) and chloroquine (CQ). Time-course fluorescence revealed that cytosolic KARS1-RFP levels gradually decreased with A23187 treatment (Fig. 4A and Supplementary Fig. 4A), while the extracellular level significantly increased following A23187 treatment and was subsequently reversed by Baf A1 and CQ (Fig. 4B and Supplementary Fig. 4B). These results indicate that KARS1 secretion is tightly associated with autophagy.

Ectopic KARS1-RFP converged to puncta co-localized with green fluorescent protein-tagged microtubule-associated proteins 1A/1B light chain 3B—an autophagosome marker—(GFP-LC3) upon serum starvation (Fig. 4C). A23187 diminished KARS1-RFP puncta co-localization with LC3 (Fig. 4D–E). The KARS1 puncta co-localized with LC3 were primarily separated from the lysosomes, whereas the KARS1-RFP non-co-localized with LC3 was co-stained with lysosomes (stained by LysoTracker; Fig. 4F), indicating that KARS1-associated autophagosomes were reduced before fusion with lysosomes. These results suggest that the overexpressed KARS1 is secreted by autophagosomes that do not fuse with lysosomes.

◀**Fig. 4**. Lysyl-tRNA synthetase 1 (KARS1) secretion occurs through autophagy. **A.** Bovine aortic endothelial cells (BAECs) were transfected with a vector containing the *KARS1* gene tagged with green fluorescent protein *(GFP)* and treated with 1 μM A23187, 250 nM bafilomycin A1 (Baf A1), or 50 μM chloroquine (CQ). Live-cell imaging was performed using a fluorescence microscope for 20 min at 1-min intervals. **B.** Quantification of KARS1 in post-culture media from BAECs transfected with a vector carrying *KARS1-V5*, pre-treated with 1 μM A23187, and 250 μM Baf A1 or 50 μM CQ. Secreted KARS1 was analyzed using two-way analysis of variance (ANOVA), followed by Tukey's honest significant difference (HSD) test ($n = 3$). **C–D.** BAECs, co-transfected with vectors carrying *KARS1*-red fluorescent protein *(RFP)* and *GFP*-microtubule-associated proteins 1A/1B light chain 3B *(LC3),* were observed under a fluorescence microscope. In **(D)**, the cells were treated with 1 μM A23187. Nuclei were counterstained with DAPI. Scale bar = 20 μm. Representative images are presented ($n = 3$). The Pearson correlation coefficients (ρ) in growth and starvation media are 0.95 ± 0.03 and 0.96 ± 0.02, respectively. **E.** The number of KARS1 puncta co-localized with LC3 in **(D)** is plotted and analyzed using one-way ANOVA, followed by Tukey's HSD test. **F.** Fluorescence microscopy images of BAECs under the same conditions as panel **(C)**. The cells were stained with LysoTracker and DAPI. Scale bar = 20 μm. Representative images are presented ($n = 3$). The Pearson correlation coefficients (ρ) for Lyso + LC3, Lyso + KARS1, and KARS1 + LC3 in growth media are 0.27, 0.78, and 0.56, respectively. In starvation media, the corresponding ρ values are 0.56, 0.86, and 0.77, respectively. All graphs are presented as mean ± SEM.

Meanwhile, signaling molecules, including AMPK and PI3K, altered by KARS1 overexpression did not affect autophagy (Supplementary Fig. 4C–E). Moreover, PI3K elevated cytosolic [Ca^{2+}] (Fig. 2F). Accordingly, these results suggest that cytosolic [Ca^{2+}] following autophagy is critical for the secretion of overexpressed (ectopic) KARS1.

Degradative autophagy reduces KARS1 secretion by degrading KARS1 within autophagosomes through lysosomal fusion

Caveolin-1 KO (Cav-1 KO) reportedly enhances autophagy[24,25]. Therefore, we examined whether Cav-1 KO increased KARS1 secretion. Unexpectedly, KARS1 was secreted by MAECs only when co-treated with A23187 and not under serum starvation. Moreover, KARS1 secretion was significantly decreased in Cav-1 KO MAECs compared with that in wild-type (WT) MAECs, although LC3 conversion was significantly increased in Cav-1 KO MAECs (Fig. 5A and Supplementary Fig. 5A).

To investigate the role of A23187 in KARS1 secretion by MAECs, we examined the association between PI3K and calcium influx (Fig. 2). The expression and phosphorylation levels of PI3K were significantly lower in MAECs than in BAECs (Fig. 5B and Supplementary Fig. 5B). A time-course experiment also showed that the maximal amount of KARS1 secreted by Cav-1 KO MAECs was two-fold lower than that secreted by WT MAECs (Fig. 5C and Supplementary Fig. 5C). Additionally, ectopic KARS1 was degraded more rapidly in Cav-1 KO cells than in WT cells (Fig. 5D and Supplementary Fig. 5D). Consistently, ectopic KARS1 in Cav-1 KO cells was more localized within lysosomes than in WT cells (Fig. 5E), and LC3 co-localized with lysosomes more extensively in Cav-1 KO cells than in WT MAECs (Fig. 5F). This suggests that KARS1 within autophagosomes is more readily exposed to degradation in Cav-1 KO cells. These high autophagy levels in Cav-1 KO cells led to the conclusion that degradative autophagy causes the rapid degradation of ectopic KARS1 rather than its extracellular secretion.

KARS1 inhibits LSS-induced cell signaling and NO production and promotes proinflammation

Next, we investigated whether the secreted KARS1 has an autocrine/paracrine function in the vascular system. To this end, BAECs were pre-treated with KARS1 in the exosomal fraction before shear exposure. KARS1 inhibited LSS-induced ERK activation (Fig. 6A).

It was previously reported that LSS-induced activation of cell signaling molecules is more dramatically enhanced than OSS-induced activation[26]. Therefore, we evaluated the effects of extracellular KARS1 on LSS-induced cell signaling molecules using recombinant KARS1. Interestingly, extracellular KARS1 dose-dependently inhibited LSS-induced activation of ERK, AKT, and eNOS (Fig. 6B and Supplementary Fig. 6A). Additionally, LSS-induced ERK activation was inhibited by KARS1 at doses lower than those required for the activation of AKT and eNOS. Moreover, 50% inhibition of ERK activation occurred at approximately 1 nM, while that of AKT and eNOS activation occurred at 10–100 nM. These findings imply that KARS1 inhibits various independent signaling pathways through differential dose effects. The inhibitory effect of KARS1 on eNOS activation was confirmed by assessing NO levels, revealing that KARS1 pre-treatment reduced LSS-induced NO production (Fig. 6C). We investigated whether KARS1 functions as a proinflammatory factor. Interestingly, KARS1 promoted the production of proinflammatory cytokines, including interleukins (IL)-1β and IL-6, without altering iNOS expression in BAECs (Supplementary Fig. 6E-F). It also enhanced leukocyte adhesion to endothelial cells (Supplementary Fig. 6G) and stimulated leukocyte chemotactic activation (Supplementary Fig. 6H). These findings suggest that KARS1 should act as a proinflammatory factor.

In addition, we found that KARS1 promoted IκB degradation (Fig. 6D and Supplementary Fig. 6B). Given that KARS1 promoted IκB degradation in BAECs to a similar extent as TNF-α, we evaluated whether secreted KARS1 impacts endothelial and smooth muscle cell apoptosis and proliferation. KARS1 induced apoptosis in BAECs, even at 10 nM, whereas no such effect was observed in rat aortic smooth muscle cells (Fig. 6E and Supplementary Fig. 6C–D). In contrast, KARS1 stimulated the proliferation of smooth muscle cells with approximately half the proliferative activity of 20% serum at 100 nM; this effect was not observed in BAECs (Supplementary Fig. 7A–B). Hence, these signaling data indicate that KARS1 acts as a cell type-specific differential regulator.

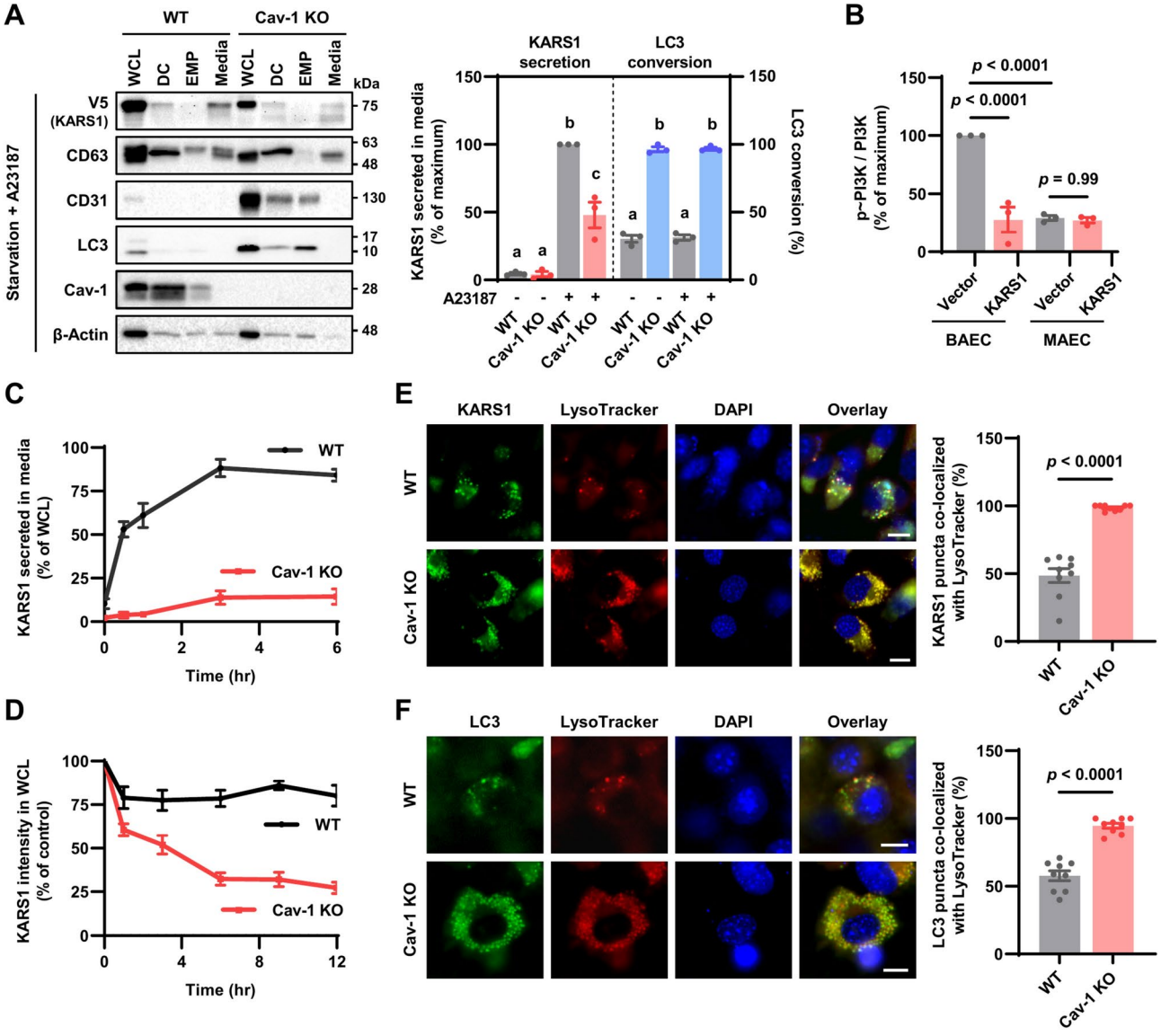

Fig. 5. Degradative autophagy diminishes lysyl-tRNA synthetase 1 (KARS1) secretion. **A.** Wild-type (WT) and caveolin-1 knock-out (Cav-1 KO) mouse aortic endothelial cells (MAECs), transfected with a vector containing the *KARS1* gene tagged with *V5*, were serum-starved for 24 h and treated with A23187 for 15 min. The post-culture media were fractionated as described in Fig. 3. Western blotting (left panel) was performed with β-Actin as the loading control. Representative blots are shown ($n = 3$). (WCL, whole-cell lysate; DC, suspended dead cells; EMP, endothelial microparticle). Quantified blot data of **(A)** and Figure S5A (right panel) analyzed using two-way analysis of variance (ANOVA) followed by Tukey's honest significant difference (HSD) test. **B.** Quantified blot data concerning PI3K and p ~ PI3K levels in bovine aortic endothelial cells and MAECs analyzed using two-way ANOVA followed by Tukey's HSD test ($n = 3$). **C.** WT and Cav-1 KO MAECs treated with 1 μM A23187 for various durations after transfection with the vector carrying *KARS1-V5* and subjected to 24 h serum starvation. **D.** WT and Cav-1 KO MAECs transfected with a vector carrying *KARS1-V5* harvested after treatment with 10 μg/ml cycloheximide (CHX). Immunoblotting was performed using an anti-V5 antibody and the results were quantified by densitometry. **E–F.** WT and Cav-1 KO MAECs, transfected with vector carrying KARS1-green fluorescent protein *(GFP)***(E)** and *GFP*-microtubule-associated proteins 1A/1B light chain 3B *(LC3)***(F),** were stained with LysoTracker and DAPI. Representative images (left panel) are presented ($n = 3$). Scale bar = 10 μm. Fluorescence images were quantified and analyzed using Student's *t*-test (right panel). In (E), the Pearson correlation coefficients (ρ) for WT and Cav-1 KO are 0.85 ± 0.03 and 0.95 ± 0.01, respectively. In (F), the corresponding ρ values for WT and Cav-1 KO are 0.92 ± 0.01 and 0.94 ± 0.01, respectively. All graphs are presented as mean ± SEM.

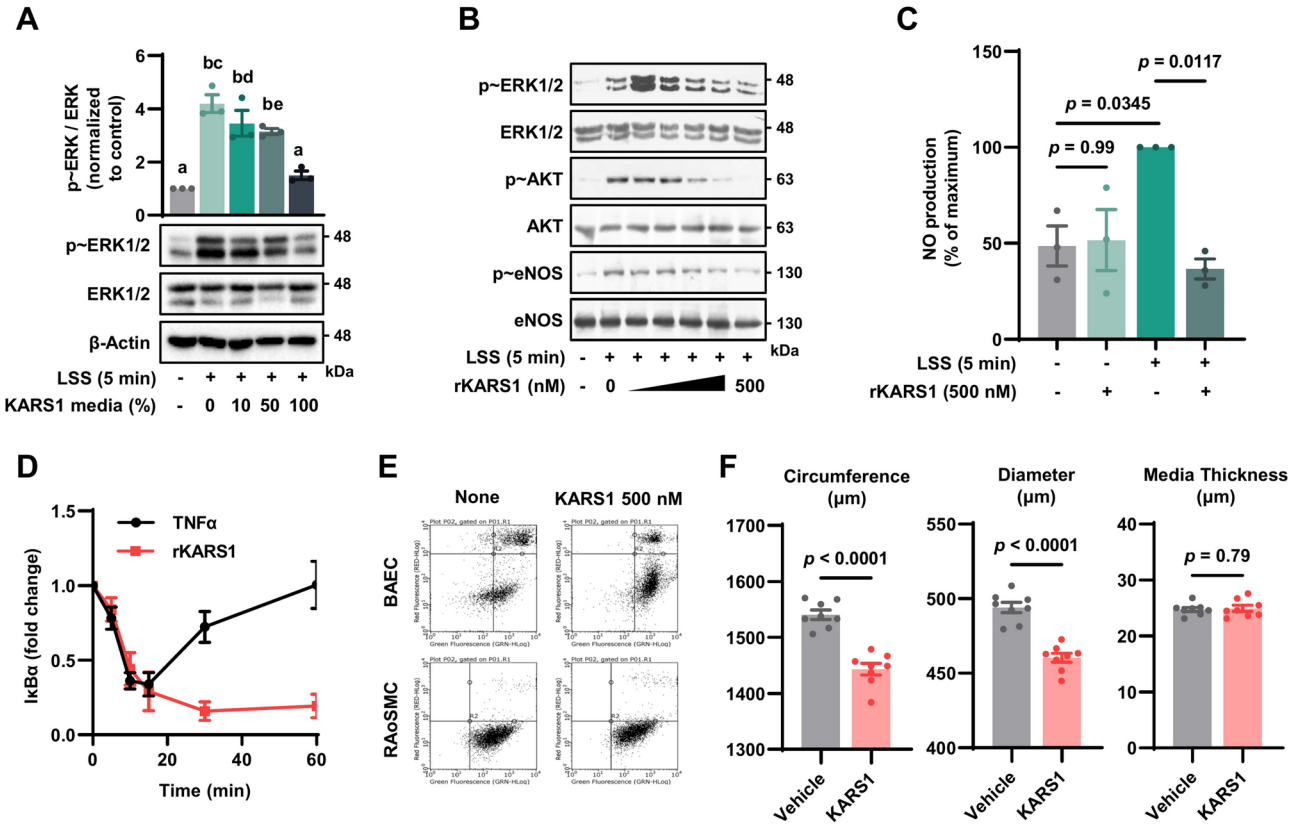

Fig. 6. Lysyl-tRNA synthetase 1 (KARS1) induces vascular alteration through impairing endothelial functions. **A.** Bovine aortic endothelial cells (BAECs) were pre-treated with post-culture media of BAECs, transfected with a vector containing the *KARS1* gene tagged with *V5*, for 1 h, and exposed to laminar shear stress (LSS). Whole-cell lysates (WCLs) were subjected to immunoblotting. β-Actin is the loading control. Representative blots are shown ($n = 3$). Quantified data (top panel) analyzed using one-way analysis of variance (ANOVA) followed by Tukey's honest significant difference (HSD) test. **B.** Serum-starved BAECs were pre-treated with recombinant KARS1 protein (His-tagged rKARS1) for 1 h and exposed to LSS. Western blotting (left panel) performed on WCLs. Representative blots are shown ($n = 3$). **C.** rKARS1-pretreated or untreated BAECs exposed to LSS. Nitric oxide (NO) levels analyzed using two-way ANOVA, followed by Tukey's HSD test ($n = 3$). **D.** BAECs were treated with 10 ng/ml TNF-α or 500 nM rKARS1. Western blot signals quantified on a line graph by densitometry. **E.** BAECs and rat aortic smooth muscle cells (RAoSMCs) were stained with Annexin V and propidium iodide after pre-treatment with 500 nM rKARS1 for 24 h; fluorescence measured by flow cytometry. **F.** Apolipoprotein E knock-out (ApoE KO) mice were fed a high-fat diet and injected with rKARS1 or phosphate buffered saline (PBS) via the tail vein once weekly for three weeks. Quantified data show the thickness of the tunica media and the circumference and diameter of carotid artery ($n = 8$; Student's *t*-test). All graphs are presented as mean ± SEM.

KARS1 decreases carotid artery diameter

To elucidate the remodeling effect of KARS1 on the carotid artery, we administered 9.6 μg KARS1 per 1 g body weight or vehicle control to ApoE KO mice via the tail vein once weekly for three weeks, followed by hematoxylin and eosin (H&E) staining of the aortic arch and carotid arteries (Fig. 6F and Supplementary Fig. 8A). The circumference of the carotid arteries of KARS1-administered mice was significantly smaller than that of vehicle-treated mice (vehicle: 1540.3 ± 23.6 μm, KARS1: 1443.3 ± 29.3 μm). The carotid artery diameters calculated based on circumference measurements also showed a significant difference (vehicle: 494.0 ± 9.8 μm, KARS1: 460.0 ± 8.6 μm). However, there was no significant difference in the medial thickness of the carotid arteries between vehicle control and KARS1-administered mice (vehicle: 24.6 ± 1.8 μm, KARS1: 24.5 ± 1.8 μm). Together, we concluded that KARS1 induced vascular remodeling through inhibitory effect on LSS-induced vascular endothelial functions.

Discussion

The primary findings of this study can be summarized as follows: (1) intracellular KARS1 overexpression is induced by OSS and (2) is secreted by autophagy stimulation in the presence of Ca^{2+}; (3) secreted KARS1 blocks LSS-induced NO production and induces cell apoptosis in endothelial cells, (4) while promoting cell proliferation in smooth muscle cells, (5) ultimately decreasing the diameter of carotid arteries. These findings raise multiple questions regarding the roles of KARS1 in vascular biology and, more importantly, the pathological

or physiological consequences of extracellular KARS1 in the vascular system. Collectively, the simultaneous presence of three stimuli—OSS, autophagy, and increased Ca^{2+} levels—may synergistically promote atherogenesis in the vascular system, even though each stimulus alone does not exert a significant effect.

OSS upregulated KARS1 expression in endothelial cells. Consequently, more KARS1 molecules than the stoichiometric amount in MSC exist in free form in the cytoplasm. Previous studies have shown that KARS1, when dissociated from MSC, is secreted into exosomes via multivesicular bodies (MVBs)[12,27]. Hence, the excess free-form KARS1 may be secreted from endothelial cells exposed to OSS. Two fates for excess KARS1 were defined in this study under autophagic stimulation: at low Ca^{2+} levels, autophagy leads to the degradation of excess KARS1, whereas increased intracellular Ca^{2+} induces its secretion. Given the critical role of Ca^{2+} in secretory vesicle fusion, it is reasonable to assume that Ca^{2+} is an essential autophagy-induced KARS1 secretion regulator. However, the detailed mechanism through which Ca^{2+} regulates this process remains unclear. KARS1 overexpression inhibited the increase in intracellular [Ca^{2+}] induced by PI3K activation, indicating that KARS1 upregulation induced degradative autophagy. Accordingly, autophagy-associated KARS1 secretion was stimulated by Ca^{2+} entry into the cytosol, mediated by PI3K activation in the presence of Cav-1. Preconditioning with a high level of degradative autophagy, as in Cav-1 KO cells, promoted KARS1 degradation in endothelial cells, diminishing its secretion. In either case, cellular damage can be prevented, but the extracellular physiological consequences differ significantly. Cellular momentum driving KARS1 secretion leads to a pro-inflammatory process in the vascular system because secreted KARS1 induces IκB degradation (*see* Fig. 6) and interleukins 6 and 1β production by leukocytes (*see* Supplementary Fig. 6F)[6].

Secreted KARS1 was found to act via an autocrine/paracrine mechanism, requiring the direct interaction between secreted KARS1 and target cell receptors. Secreted KARS1 in endothelial cells is largely similar to that in cancer cells; however, the detailed processes of secretion and the specific forms of secreted KARS1 differ. In cancer cells, caspase-8, activated by starvation, truncates KARS1, leading to its dissociation from MSC and binding to syntenin. The KARS1–syntenin complex is then translocated to MVBs, where it is packaged into exosomes for secretion. Following secretion and subsequent exosome rupture, KARS1 is exposed to the extracellular space, where it binds to target cells[12,27]. However, in endothelial cells, the overexpressed and free forms of KARS1 are secreted via autophagy induction in the presence of Ca^{2+} and become externally exposed as exosome-adhering molecules (*see* Fig. 3). Therefore, KARS1 secreted by endothelial cells can facilitate direct interactions with target cell receptors. Based on the secreted form of KARS1, we propose a model in which KARS1 is initially encapsulated by autophagosomes, which then fuse with exosome-containing MVBs to form amphisomes. Finally, KARS1-associated exosomes are secreted via membrane fusion between amphisomes and the plasma membrane (*see* Model figure; Supplementary Fig. 5E).

The data obtained herein provide insights into the pathological roles of secreted KARS1 in vascular biology. First, the inhibitory effect of KARS1 on LSS-induced NO production implies that KARS1 has pathological implications, given that reduced NO levels and disrupted LSS are well-accepted to be atherogenic[15,19]. Consistent with previous studies showing that KARS1 acts as a pro-inflammatory agent[6] and a microphthalmia-associated transcription factor upon immunological challenge[4], secreted KARS1 in the vascular system has also been proposed to contribute to vascular pathology, including atherosclerosis development because inflammatory processes are early events in atherosclerotic plaque formation[13,14]. KARS1 overexpression in areas of vessels exposed to OSS, a known pro-atherogenic factor (*see* Fig. 1C), and in partially ligated carotids forming atherosclerotic plaques (*see* Fig. 1A) suggests an association with vascular pathology. In this study, KARS1 secretion was induced by autophagy stimulation in the presence of Ca^{2+}. Thus, considering that autophagy plays an important role in plaque development[28], our observations suggest that KARS1 might act as an atherogenic factor. Moreover, secreted KARS1 appears to promote endothelial cell apoptosis. Although the pathological role of endothelial cell apoptosis remains controversial, the pro-apoptotic activity of KARS1 is considered to partially contribute to vascular disease development based on the relationship among apoptosis, plaque rupture, and atherothrombosis[29]. In summary, the notion that KARS1 acts as an atherogenic factor is supported by the following findings: (1) KARS1 is overexpressed in atheroprone regions; (2) KARS1 secretion is associated with autophagy (a prognostic factor for atherosclerosis) and intracellular [Ca^{2+}]; (3) secreted KARS1 inhibits LSS (an anti-atherogenic factor)-induced NO production; (4) secreted KARS1 alters vessel diameter by regulating endothelial functions (*see* Model figure; Supplementary Fig. 8B).

The in vitro inhibitory effect of KARS1 on LSS-induced NO production (*see* Fig. 6C) may partially account for the in vivo results (*see* Fig. 6F), as KARS1 potentially blocked LSS-induced vasodilation, leading to a reduced carotid diameter. However, KARS1 is not secreted under normal physiological conditions. A previous publication has shown that various cancer cell lines secret KARS1 into extracellular spaces upon TNF-α stimulation or starvation[6,12]. Accordingly, most KARS1 proteins may be present in the MSC of normal or quiescent vascular cells. Under such conditions, although endothelial cells are stimulated by autophagy induction in the presence of Ca^{2+}, KARS1 cannot be secreted due to its association with MSC. Consequently, our observation of OSS-induced KARS1 overexpression strongly supports the notion that KARS1 exists in a free form in the cytosol and is secreted into extracellular spaces under secretory stimulation.

One limitation of this study is that the in vitro efficacy of KARS1 was not replicated in vivo. The comparatively insignificant results from the mouse experiments could be due to (1) the difference between recombinant KARS1 and exosome-associated KARS1, (2) the distinction between systemically circulating KARS1 injected intravenously and locally acting paracrine KARS1 secreted from the endothelium, and (3) the use of an inappropriate animal model for intravenous injection. In the future, we aim to identify a more suitable animal model to validate our in vitro findings.

In conclusion, our findings support the notion that KARS1 plays a crucial role in vascular physiology or pathophysiology through OSS-induced KARS1 overexpression, Ca^{2+}/autophagy-stimulated KARS1 secretion, attenuation of endothelial responses to LSS, and remodeling of the tunica media. Pro-atherogenic functions of

KARS1 are closely linked to its pro-inflammatory activity. Hence, these findings reveal a dichotomy in KARS1 functions—pro-atherogenic versus pro-inflammatory—in the vascular and immune systems. At the cellular level, these bisectional activities of KARS1 possibly stem from KARS1 secretion, induced by TNF-α in cancer cells [6] and by autophagy in endothelial cells. Together, secreted KARS1, specifically present in the vascular system (circulating in the blood), exhibits pro-inflammatory and pro-atherogenic properties, suggesting its pathological role. Therefore, reducing or blocking secreted KARS1 may serve as a potential strategy for maintaining vascular and overall biomedical health.

Materials and methods

Materials

Information on plasmids, primers, chemicals, and antibodies is provided in Supplementary Tables 1–4.

Cell culture

BAECs, obtained from descending thoracic aortas as previously described[16], were cultured at 37 ℃ and 5% CO_2 in Dulbecco's modified Eagle's medium (DMEM; WELGENE, Inc., #LM001-11) supplemented with 20% fetal bovine serum (FBS; WELGENE, Inc., #S001-01) and 1% penicillin–streptomycin (WELGENE, Inc., #LS202-02). BAECs from passages 3 to 15 were used.

MAECs were obtained and cultured as previously described[30], at 37 ℃ and 5% CO_2 in DMEM containing 10% FBS, 1% penicillin–streptomycin, 0.01% endothelial cell growth supplement (Corning, Inc., #356,006), and 1 × minimum essential medium (MEM) non-essential amino acid solution (Merck, KGaA, #M7145-100ML). The MAECs used in this study were immortalized.

Rat aortic smooth muscle cells (RAoSMCs) were purchased from the Korean Cell Line Bank and cultured at 37 ℃ and 5% CO_2 in DMEM containing 10% FBS and 1% penicillin–streptomycin. RAoSMCs from passages 4 to 8 were used.

For serum starvation, all cells were cultured at 37 ℃ and 5% CO_2 in DMEM containing only 1% penicillin–streptomycin.

LSS

Glass slides containing a cell monolayer were assembled in a parallel-plate shear chamber. Non-individual LSS was generated by changing the flow rate of the serum-starved media delivered to the cells using a flow-loop system, as previously described[30].

OSS

Cells grown to 90% confluence in 100 mm culture dishes were exposed to OSS in growth media by rotating a Teflon cone (0.5° cone angle), as described previously[31]. Briefly, the cells grown in culture dishes were positioned in a cone rotating with directional flow changes at 1 Hz cycle (± 5 dyn/cm^2). The OSS was generated by rotating the cone back and forth using a stepping servomotor and computer program handmade by DC Motor Company, LLC. The cells were exposed to OSS for the indicated periods.

Recombinant KARS1 preparation

Recombinant KARS1 was obtained as previously described [6].

Animal cell transfection

Cells grown to 90% confluence were treated with a mixture of plasmid DNA (vectors carrying various genes or empty vectors at 8 μg per 100 mm culture dishes, 2 μg per 35 mm culture dishes, and 0.1 μg per 96-well plates) and polyethylenimine at a ratio of 1:10 in culture media without antibiotics, and then incubated for more than 12 h. Supplementary Table 1 lists the plasmid DNA used for transfection.

Total RNA isolation and cDNA synthesis

Total RNA was isolated from the cells using NucleoZOL. Purified total RNA was reverse-transcribed into cDNA using M-MLV reverse transcriptase, 10 mM dNTP, and DEPC-treated water. Reverse transcription was performed at 37 ℃ for 1 h, after denaturation at 70 ℃ for 5 min.

Total RNA was isolated from animals using the QIAzol and miRNeasy Mini Kit (QIAGEN, GmbH., #217,084) according to the manufacturer's protocol. Purified total RNA was reverse-transcribed into cDNA using a high-capacity RNA-to-cDNA kit (Thermo Fisher Scientific, Inc., #4,387,406) according to the manufacturer's protocol.

Quantitative real-time polymerase chain (qPCR) reaction

The reverse-transcribed cDNAs were amplified by PCR using TOPreal™ qPCR 2 × preMIX SYBR Green, 5 μM forward primer, 5 μM reverse primer, and DEPC-treated water. The PCR was performed for 35–45 cycles with the following conditions: denaturation at 95 ℃ for 10 s, annealing at 60 ℃ for 15 s, and extension at 72 ℃ for 30 s. Supplementary Table 4 lists the primers used for qPCR amplification. GAPDH mRNA and 18S ribosomal RNA were internal controls.

Preparation of cell lysates

Cells grown under optimized conditions were washed with ice-cold phosphate-buffered saline (PBS) and harvested in radioimmunoprecipitation assay lysis buffer (150 mM NaCl, 1% NP-40, 0.5% sodium deoxycholate, 0.1% sodium dodecyl sulfate (SDS), and 50 mM Tris–HCl, pH 8.0) containing 1 mM phenylmethylsulfonyl fluoride (PMSF) and 10 mM sodium orthovanadate. The soluble lysates were separated by centrifugation at

10,000 × *g* for 15 min. Total protein amounts in the cell lysates were determined using a Micro BCA™ Protein Assay Kit (Thermo Fisher Scientific, Inc., #23,235).

Exosome isolation of post-culture media

Exosomes were isolated from the post-culture media using the Total Exosome Isolation Reagent. The harvested culture media were mixed with the reagent at a 2:1 ratio and incubated overnight. Exosomes were isolated by centrifugation at 10,000 × *g* for 1 h. The isolated exosomes were resuspended in PBS.

Fractionation of post-culture media

The media in which the cells were cultured were harvested and separated by differential centrifugation. First, the dead cells (referred to as "DC" in figures) were separated from harvested media by centrifugation at 500 × *g* for 10 min. Second, the cell debris (not shown) was separated by centrifugation at 10,000 × *g* for 30 min. Third, the endothelial microparticles (referred to as "EMP" in figures) were separated by ultracentrifugation at 100,000 × *g* for 90 min using an Optima L-90 K Ultracentrifuge (Beckman Coulter, Inc.) and SW 41 Ti swinging-bucket rotor (Beckman Coulter, Inc., #331,362). The separated EMPs were washed by ultracentrifugation at 100,000 × *g* for 90 min with PBS containing 1 mM PMSF and 1 × Halt™ Protease Inhibitor Cocktail. The remaining solutions are referred to as "media" in the figures.

Sucrose density gradient fractionation

Sucrose density gradient fractionation was performed using media obtained from the centrifugal fractionation method. A total of 2 ml of 90% sucrose solution was placed at the bottom of the tube, followed by 4 ml of 20% sucrose solution, and 4 ml of the supernatant was layered on top. The solution was centrifuged at 100,000 × *g* for 16 h using an Optima L-90 K Ultracentrifuge (Beckman Coulter, Inc.) and an SW 41 Ti swinging-bucket rotor (Beckman Coulter, Inc., #331,362). After centrifugation, the solution was separated into 1 ml fractions starting from the top, with the upper fraction being fraction 1 and the lower fraction being fraction 10 (referred to as "F1" to "F10" in figures).

Co-IP

Co-IP was performed using two groups of antibodies: immunoglobulin G (IgG; control) and the target antibody. This assay was performed using cell lysates and post-culture media. For Co-IP with cell lysates, 500 µg of soluble protein was mixed with 2 µg of antibody. Moreover, in post-culture media, 1.5 ml of media was mixed with 2 µg of antibody for each sample. The mixture was incubated overnight before adding 80 µl of Protein A/G PLUS-Agarose and mixing by slow rotation for 3 h. To precipitate the agarose beads, the mixtures were centrifuged at 1,200 × *g* for 5 min. The supernatant was removed, and the pellet was thoroughly washed with PBS containing 1 mM PMSF by centrifugation at 1,200 × *g* for 3 min.

Western blotting

Soluble proteins were resolved by 7.5–15% SDS–polyacrylamide gel electrophoresis (PAGE), transferred to a polyvinylidene fluoride membrane (Merck, KGaA., #IPVH00010), and blotted with primary antibodies diluted in 2% bovine serum albumin (BSA) overnight. Subsequently, the membranes were incubated with horseradish peroxidase-conjugated secondary antibodies for 1 h and developed with a ChemiDoc XRS + imaging system (Bio-Rad Laboratories, Inc.) using an enhanced chemiluminescence detection method (Amersham Piscataway, NJ, USA). The results were analyzed and quantified using the Image Lab software version 6.1 (Bio-Rad Laboratories, Inc.).

In cases that did not require western blot, samples were stained with Coomassie brilliant blue staining solution (1% Pierce™ Coomassie Brilliant Blue Dyes, 10% acetic acid, 50% methanol) for 3 h after SDS-PAGE, and destained with destaining solution (3% glycerol, 10% acetic acid, 40% methanol). Imaging was performed using the same system as previously described.

Fluorescence microscopy

For fluorescence microscopy, cells were seeded on coverslips and cultured to 60% confluence. If necessary, experiments were conducted 24 h after transfection. Coverslips were washed twice with PBS, and the cells were fixed with 4% paraformaldehyde at room temperature for 10 min. The fixed coverslips were transferred to glass slides after mounting with VECTASHIELD® Antifade Mounting Medium with DAPI (4′,6-diamidino-2-phenylindole) and observed using the EVOS™ M5000 Imaging System (Thermo Fisher Scientific, Inc.).

For immunocytochemistry, the cells were permeabilized with 0.25% Triton X-100 after fixation and incubated overnight with the target primary antibodies diluted in 2% BSA. The cells were then treated with goat anti-mouse IgG (H + L), a highly cross-adsorbed secondary antibody, for 1 h. Images were analyzed as previously described.

Ca^{2+} quantification in cytoplasm

Cells grown to approximately 80% confluence in a black 96-well plate (CELL CULTURE MICROPLATE, 96 WELL, PS, F-BOTTOM; Greiner Bio-One, GmbH., #655,086) were incubated with 1 µM Fura-2, AM diluted in calcium-free PBS for 30 min in 37 ℃ and 5% CO_2. The cells were washed with PBS and incubated for 30 min in a serum-starved media, as previously described. Fluorescence was detected with excitation at 360 ± 40 nm and emission at 528 ± 20 nm using a Synergy HTX Multimode Microplate Reader (Agilent Technologies, Inc.) and Gen5 software version 3.16.10 (Agilent Technologies, Inc.).

NO quantification

Cellular NO level was quantified using the fluorescence spectrum of intracellular DAF-2 DA (4,5-Diaminofluorescein diacetate). Cells were pre-incubated with a hydroxyethyl piperazine ethane sulfonicacid (HEPES) buffer (5 mM HEPES, 140 mM NaCl, 5 mM KCl, 2 mM $CaCl_2$, 1 mM $MgCl_2$, 5 mM Glucose, pH7.4) containing 1 μM A23187 for 20 min at 37 ℃. Subsequently, cells were incubated at 37 °C and 5% CO_2 with 0.1 μM DAF-2 for 15 min, harvested, and lysed by sonication. Supernatants were then obtained by centrifugal fractionation, diluted, and scanned using an RF 5301PC (Shimadzu, Co.) with excitation at 495 nm and emission at 515 nm. NO levels were calculated from the DAF-2 fluorescence intensity.

Fluorescence-activated cell sorting analysis

Cells cultured at 37 ℃ and 5% CO_2 were washed with PBS twice and detached from the culture dish using 1 × Trypsin-Ethylenediaminetetraacetic acid (WELGENE, Inc., #LS015-02). The cell suspension was centrifuged at 2,000 × *g* for 5 min, and the supernatant was removed. The cells were then washed with PBS by centrifugation at 2,000 × *g* for 5 min; this washing step was repeated twice. The subsequent process was performed using an ApoScan kit (Annexin V-FITC detection kit; Biobud, Co., Ltd., #LS-02–100) according to the manufacturer's instructions. After adding 3 μM propidium iodide, fluorescence detection was performed using a Guava® easyCyte HT System (Merck, KGaA) and the GuavaSoft software version 3.1 (Merck, KGaA).

Chemotaxis assay

Chemotactic effect of THP-1 cells was assessed using the QCM Chemotaxis Cell Migration Assay (Merck, KGaA, #ECM508) following the manufacturer's protocol.

Cell proliferation

Cell proliferation was measured using EZ-Cytox (DoGen Bio, Co., Ltd., #EZ-3000) as previously described [32]. Briefly, cells subjected to the experimental conditions were washed twice with PBS and incubated withe WST-1 reagent. The absorbance of live cells was measured at 450 nm using a model 550 Microplate Reader (Bio-Rad Laboratories, Inc.).

Nuclear fragmentation assay

Cells were cultured to confluence on coverslips and subjected to the experimental conditions. Subsequently, cells were fixed with 4% paraformaldehyde and stained with Hoechst 33,258 solution. The cells were imaged using a Zeiss Axioplan 2 microscope (Carl Zeiss, AG) and the Axiovision SE64 software version 4.9.1 (Carl Zeiss, AG). For comparison, cells were imaged in the bright-field and fluorescence channels at the same magnification.

Animal studies with carotid artery partial ligation

All animal studies were performed using 6- to 8-week-old male ApoE KO mice. ApoE KO mice were obtained from Central Lab Animal, Inc., and partial ligation was performed as previously described[33]. Briefly, three of the four caudal branches of the LCA (left external carotid, internal carotid, and occipital arteries) were ligated using a 6–0 silk suture, while the superior thyroid artery and RCA were left intact. Mice were fed a high-fat diet immediately after partial ligation and sacrificed after 2 weeks. Animals were anaesthetized with 3.5% isoflurane initially; this dose was then reduced to 1.5–2% during the entire procedure of partial ligation of the LCA. Mice were sacrificed by CO_2 inhalation.

Immunohistochemistry staining

Cryo-Sects. (5 μm) from partially carotid-ligated mice were fixed in 10% formalin for 10 min and blocked with peroxide block for 10 min at room temperature. Each section was incubated with the target primary antibody for 1 h at room temperature. Following incubation, a Polink-2 Plus HRP Broad Spectrum DAB Detection Kit (OriGene Technologies, Inc., # D41-18) was used to visualize the antibodies. The sections were counterstained with hematoxylin or Oil Red O. Detailed experimental procedures were previously described[33]. Images were obtained using an Olympus BX51 Fluorescence Microscope (Olympus, Co.).

En face staining

For *en face* staining, the mice were euthanized by CO_2 inhalation, and the aortas were pressure-fixed with saline containing 10% formalin. The aortas were carefully cleaned in situ, and the arches and thoracic aortas were dissected and stained with the target primary antibody, followed by incubation with rhodamine-conjugated secondary antibodies for 2 h at room temperature. The aortas were opened, and the LC and GC of each arch and innominate artery were separated. The detailed procedures were performed as previously described [34]. The aortas and carotid arteries were then mounted on glass slides with VECTASHIELD® Antifade Mounting Medium with DAPI. *En face* images were obtained using a Zeiss LSM 510-META confocal laser scanning microscope (Carl Zeiss, AG) and LSM 5 software (www.zeiss.de/lsm, Carl Zeiss, AG).

Measurement of carotid geometry in KARS1-administered mice

Ten-week-old male ApoE KO mice were purchased from Central Lab. Animal Inc. The mice were fed a high-fat diet and treated with KARS1 (9.6 μg/mouse g) via tail-vein injection once weekly for three weeks. The control group was injected with PBS. After three weeks, all mice were sacrificed. Carotid tissues were quickly processed for fixation with Tissue-Tek® O.C.T. Compound and stored at − 80 °C until use. The tissues were cryo-sectioned at 5 μm thickness and stained with H&E and Oil Red O. Images of the carotids were captured using an Olympus BX51 Fluorescence Microscope (Olympus, Co.), and the thickness, circumference, and diameter of the carotids were measured and calculated using the NIH Image J software version 1.54 h (https://imagej.net/ij/).

Quantification and statistical analysis

Data were obtained from at least three independent experiments. Graphical representations and statistical analyses were performed using GraphPad Prism 8.4.3, and the data are presented as the mean ± standard error of the mean (SEM). The statistical significance of the experimental results was assessed using Student's *t*-test and one-way or two-way analysis of variance (ANOVA) followed by Tukey's honest significant difference (HSD) test, Sidak's correction, and Dunnett's multiple comparison test. *P*-values < 0.05 were considered significant.

Data availability

All data supporting our research are available upon reasonable request. For further information requests, please contact corresponding author (heonyong@dankook.ac.kr). All supporting materials in this study are described in the Supplementary Informations.

Received: 7 December 2024; Accepted: 25 March 2025
Published online: 01 April 2025

References

1. Park, S. G., Choi, E. C. & Kim, S. Aminoacyl-tRNA synthetase–interacting multifunctional proteins (AIMPs): A triad for cellular homeostasis. *IUBMB Life* **62**, 296–302 (2010).
2. Kovaleski, B. J. et al. In vitro characterization of the interaction between HIV-1 gag and human lysyl-tRNA synthetase. *J. Bio. Chem.* **281**, 19449–19456 (2006).
3. Carmi-Levy, I. et al. Importin beta plays an essential role in the regulation of the LysRS-Ap(4)A pathway in immunologically activated mast cells. *Mol. Cell. Biol.* **31**, 2111–2121 (2011).
4. Yannay-Cohen, N. et al. LysRS serves as a key signaling molecule in the immune response by regulating gene expression. *Mol. Cell* **34**, 603–611 (2009).
5. Ofir-Birin, Y. et al. Structural switch of lysyl-tRNA synthetase between translation and transcription. *Mol. Cell* **49**, 30–42 (2013).
6. Park, S. G. et al. Human lysyl-tRNA synthetase is secreted to trigger proinflammatory response. *Proc. Natl. Acad. Sci. USA* **102**, 6356–6361 (2005).
7. Kim, D. G. et al. Interaction of two translational components, lysyl-tRNA synthetase and p40/37LRP, in plasma membrane promotes laminin-dependent cell migration. *FASEB J.* **26**, 4142–4159 (2012).
8. Kaminska, M. et al. Dynamic organization of aminoacyl-tRNA synthetase complexes in the cytoplasm of human cells. *J. Biol. Chem.* **284**, 13746–13754 (2009).
9. Kang, T. et al. AIMP3/p18 controls translational initiation by mediating the delivery of charged initiator tRNA to initiation complex. *J. Mol. Biol.* **423**, 475–481 (2012).
10. Park, S. G. et al. Precursor of pro-apoptotic cytokine modulates aminoacylation activity of tRNA synthetase. *J. Biol. Chem.* **274**, 16673–16676 (1999).
11. Abrahamsen, H. & Stenmark, H. Protein secretion: Unconventional exit by exophagy. *Curr. Biol.* **20**, R415–R418 (2010).
12. Kim, S. B. et al. Caspase-8 controls the secretion of inflammatory lysyl-tRNA synthetase in exosomes from cancer cells. *J. Cell Biol.* **216**, 2201–2216 (2017).
13. Dinarello, C. A. Anti-inflammatory agents: Present and future. *Cell* **140**, 935–950 (2010).
14. Weber, C. & Noels, H. Atherosclerosis: Current pathogenesis and therapeutic options. *Nat. Med.* **17**, 1410–1422 (2011).
15. Malek, A. M., Alper, S. L. & Izumo, S. Hemodynamic shear stress and its role in atherosclerosis. *JAMA* **282**, 2035–2042 (1999).
16. Park, H. et al. Plasma membrane cholesterol is a key molecule in shear stress-dependent activation of extracellular signal-regulated kinase. *J. Biol. Chem.* **273**, 32304–32311 (1998).
17. Jo, H. et al. Differential effect of shear stress on extracellular signal-regulated kinase and N-terminal Jun kinase in endothelial cells. Gi2- and Gbeta/gamma-dependent signaling pathways. *J. Biol. Chem.* **272**, 1395–1401 (1997).
18. Go, Y. M. et al. Phosphatidylinositol 3-kinase gamma mediates shear stress-dependent activation of JNK in endothelial cells. *Am. J. Physiol.* **275**, H1898–H1904 (1998).
19. Zhang, Y. et al. AMP-activated protein kinase is involved in endothelial NO synthase activation in response to shear stress. *Arterioscler. Thromb. Vasc. Biol.* **26**, 1281–1287 (2006).
20. Cook, S. Coronary artery disease, nitric oxide and oxidative stress: The "Yin-Yang" effect-a Chinese concept for a worldwide pandemic. *Swiss Med. Wkly.* **136**, 103–113 (2006).
21. Frank, P. G. & Lisanti, M. P. Role of caveolin-1 in the regulation of the vascular shear stress response. *J. Clin. Invest.* **116**, 1222–1225 (2006).
22. Cooke, J. P. NO and angiogenesis. *Atheroscler. Suppl.* **4**, 53–60 (2003).
23. Suo, J. et al. Hemodynamic shear stresses in mouse aortas: Implications for atherogenesis. *Arterioscler. Thromb. Vasc. Biol.* **27**, 346–351 (2007).
24. Shiroto, T. et al. Caveolin-1 is a critical determinant of autophagy, metabolic switching, and oxidative stress in vascular endothelium. *PLoS ONE* **9**, e87871 (2014).
25. Zhang, X. et al. Cav-1 (Caveolin-1) deficiency increases autophagy in the endothelium and attenuates vascular inflammation and atherosclerosis. *Arterioscler. Thromb. Vasc. Biol.* **40**, 1510–1522 (2020).
26. Guo, D., Chien, S. & Shyy, J. Y. Regulation of endothelial cell cycle by laminar versus oscillatory flow: Distinct modes of interactions of AMP-activated protein kinase and Akt pathways. *Circ. Res.* **100**, 564–571 (2007).
27. Kim, S. B., Cho, S. & Kim, S. Exosomal secretion of truncated cytosolic lysyl-tRNA synthetase induces inflammation during cell starvation. *Cell Stress.* **2**, 119–121 (2018).
28. Ni, D., Mo, Z. & Yi, G. Recent insights into atherosclerotic plaque cell autophagy. *Exp. Biol. Med. (Maywood)* **246**, 2553–2558 (2021).
29. Napoli, C. Oxidation of LDL, atherogenesis, and apoptosis. *Ann. NY Acad. Sci.* **1010**, 698–709 (2003).
30. Kim, J. et al. X-linked inhibitor of apoptosis protein controls alpha5-integrin-mediated cell adhesion and migration. *Am. J. Physiol. Heart Circ. Physiol.* **299**, H300–H309 (2010).
31. Sorescu, G. P. et al. Bone morphogenic protein 4 produced in endothelial cells by oscillatory shear stress stimulates an inflammatory response. *J. Biol. Chem.* **278**, 31128–31135 (2003).
32. Weir, L., Robertson, D., Leigh, I. M. & Panteleyev, A. A. The reduction of water-soluble tetrazolium salt reagent on the plasma membrane of epidermal keratinocytes is oxygen dependent. *Anal. Biochem.* **414**, 31–37 (2011).
33. Nam, D. et al. Partial carotid ligation is a model of acutely induced disturbed flow, leading to rapid endothelial dysfunction and atherosclerosis. *Am. J. Physiol. Heart Circ. Physiol.* **297**, H1535–H1543 (2009).
34. Zhou, J., Lhoták, S., Hilditch, B. A. & Austin, R. C. Activation of the unfolded protein response occurs at all stages of atherosclerotic lesion development in apolipoprotein E-deficient mice. *Circulation* **111**, 1814–1821 (2005).

Acknowledgements
The Schematic diagrams were created with BioRender.com (Yun, K. (2025) BioRender.com/c30x864 & Yun, K. (2025) BioRender.com/t75w675). We would like to thank Editage (www.editage.co.kr) for English language editing.

Author contributions
K.Y, Y.S, Y.O, H.S.M, J.G.C designed and performed in vitro experiments. S.K, Y.B.S, D.J.S, K.K, designed and performed in vivo experiments. S.K, H.J, H.P contributed to methodology and conceptualization. H.P supervised the overall study and drafted the manuscript. All authors contributed to the article and approved the submitted version.

Funding
This study was supported by the Basic Science Research Program of the National Research Foundation of Korea and was funded by the Korea government (MSIT) (NRF-2016R1D1A1B02007197 & NRF-2021R1A3B1076605).

Declarations

Competing interests
The authors declare no competing interests.

Ethics approval
All animal studies in this research were approved by the Animal Use Committee of Ewha Womans University (ESM-12–0191) and Chungbuk National University (CBNUA-2242–24-02). This study was performed in accordance with relevant guidelines and regulations. All methods are reported in accordance with ARRIVE guidelines.

Consent for publication
All authors involved in this study have confirmed and approved the final manuscript.

Additional information
Supplementary Information The online version contains supplementary material available at https://doi.org/10.1038/s41598-025-96046-y.

Correspondence and requests for materials should be addressed to H.P.

Reprints and permissions information is available at www.nature.com/reprints.

Publisher's note Springer Nature remains neutral with regard to jurisdictional claims in published maps and institutional affiliations.